

Detecting the Neutrino Mass Hierarchy with a Supernova at IceCube

Amol S. Dighe, Mathias Th. Keil and Georg G. Raffelt

Max-Planck-Institut für Physik (Werner-Heisenberg-Institut)
Föhringer Ring 6, 80805 München, Germany

Abstract. IceCube, a future km^3 antarctic ice Cherenkov neutrino telescope, is highly sensitive to a galactic supernova (SN) neutrino burst. The Cherenkov light corresponding to the total energy deposited by the SN neutrinos in the ice can be measured relative to background fluctuations with a statistical precision much better than 1%. If the SN is viewed through the Earth, the matter effect on neutrino oscillations can change the signal by more than 5%, depending on the flavor-dependent source spectra and the neutrino mixing parameters. Therefore, IceCube together with another high-statistics experiment like Hyper-Kamiokande can detect the Earth effect, an observation that would identify specific neutrino mixing scenarios that are difficult to pin down with long-baseline experiments. In particular, the normal mass hierarchy can be clearly detected if the third mixing angle is not too small, $\sin^2 \theta_{13} \gtrsim 10^{-3}$. The small flavor-dependent differences of the SN neutrino fluxes and spectra that are found in state-of-the-art simulations suffice for this purpose. Although the absolute calibration uncertainty at IceCube may exceed 5%, the Earth effect would typically vary by a large amount over the duration of the SN signal, obviating the need for a precise calibration. Therefore, IceCube with its unique geographic location and expected longevity can play a decisive role as a “co-detector” to measure SN neutrino oscillations. It is also a powerful stand-alone SN detector that can verify the delayed-explosion scenario.

1. Introduction

The antarctic neutrino telescope AMANDA [1, 2] and the future km^3 IceCube [3, 4] are designed to observe high-energy neutrinos from astrophysical sources. The ice is instrumented with photomultipliers to pick up the Cherenkov light from secondary charged particles. In order to reach the large volume needed to detect the expected small fluxes at high energies, the density of optical modules is far too sparse to measure, for example, solar neutrinos. However, it has been recognized for a long time that these instruments can detect a supernova (SN) neutrino burst because the Cherenkov glow of the ice can be identified as time-correlated noise among all phototubes [5, 6]. This approach has been used by AMANDA to exclude the occurrence of a galactic SN over a recent observation period [7].

For AMANDA the physics potential of a possible SN observation is essentially limited to its detection, notably in the context of the Supernova Early Warning System

(SNEWS) that would alert the astronomical community several hours before the optical explosion [8, 9]. For the future IceCube with 4800 optical modules, however, the number of detected Cherenkov photons would be of order 10^6 and thus so large that several interesting physics questions could be addressed in earnest.

The observed quantity is the number of Cherenkov photons caused by the SN neutrinos as a function of time, i.e. a measure of the energy deposited by the neutrinos in the ice. Therefore, the information about the SN signal is far more limited than what can be extracted from a high-statistics observation in Super-Kamiokande or other low-energy experiments that detect individual events. However, galactic SNe are so rare, perhaps a few per century, that the chances of observing one depend crucially on the long-term stability of the neutrino observatories. Once IceCube has been built it may well operate for several decades, backing up the low-energy experiments. Besides the detection and associated early warning one could measure important details of the neutrino light-curve, for example the existence and duration of the initial SN accretion phase, the overall duration of the cooling phase, and so forth. Such an observation would provide a plethora of astrophysically valuable information.

However, from the perspective of neutrino physics a *simultaneous* observation in both IceCube and another large detector such as Super-Kamiokande or Hyper-Kamiokande would be especially useful. Assuming that the neutrinos have traversed significantly different paths through the Earth, the two signals could well show measurable differences caused by neutrino oscillations in matter [10, 11, 12, 13, 14]. As this Earth effect shows up only for certain combinations of neutrino mixing parameters, a dual observation may well distinguish, for example, between the normal and inverted neutrino mass hierarchy. It is well known that observing SN neutrinos with two or more detectors with different Earth-crossing lengths is extremely useful, but IceCube’s potential has not been explored in this context. With all the low-energy observatories being in the northern hemisphere, IceCube’s location in Antarctica is uniquely complementary for this purpose.

Any oscillation signature depends on the small flavor-dependent differences between the fluxes and spectra at the source. If these differences were as large as had been assumed until recently there would be little question about IceCube’s usefulness for co-detecting the Earth effect. However, a more systematic study of the flavor-dependence of the SN neutrino fluxes and spectra reveals that these differences are more subtle, although by no means negligible [15, 16, 17, 18]. We evaluate IceCube’s potential as a co-detector from the perspective of these “pessimistic” assumptions about the primary fluxes and spectra.

This paper is organized as follows. In Sec. 2, we show that the neutrino signal from a galactic supernova can be measured at IceCube with a sub-percent statistical precision. In Sec. 3, we calculate the Earth matter effects on this signal and illustrate that it is possible to detect them in conjunction with another high statistics experiment. Sec. 4 concludes.

2. Supernova Neutrino Detection in Ice Cherenkov Detectors

2.1. Cherenkov Photons in One Optical Module

The SN neutrinos streaming through the antarctic ice interact according to $\bar{\nu}_e p \rightarrow n e^+$ and some other less important reactions. The positrons, in turn, emit Cherenkov light that is picked up by the optical modules (OMs) frozen into the ice. While the expected number of detected photons per OM was calculated in Refs. [5, 6], we revisit their estimate for two reasons. First, the SN signal was directly scaled to the historical SN 1987A observation in Kamiokande II so that the exact assumptions about the neutrino flux are not directly apparent. Second, the expected number of Cherenkov photons detected by one OM was based on estimating an effective ice volume seen by one OM. However, it is much simpler to work in the opposite direction and start with the homogeneous and isotropic Cherenkov glow of the ice caused by the SN neutrinos. The OM is immersed in this diffuse bath of photons and picks up a number corresponding to its angular acceptance and quantum efficiency.

As a first simplification we limit ourselves to the signal caused by the inverse β reaction $\bar{\nu}_e p \rightarrow n e^+$. The $\bar{\nu}_e$ fluence (time-integrated flux) at Earth is

$$\mathcal{F}_{\bar{\nu}_e} = 1.745 \times 10^{11} \text{ cm}^{-2} f_{\text{SN}}. \quad (1)$$

We define the “SN fudge factor” as

$$f_{\text{SN}} \equiv \frac{E_{\bar{\nu}_e, \text{tot}}}{5 \times 10^{52} \text{ erg}} \frac{15 \text{ MeV}}{\langle E_{\bar{\nu}_e} \rangle} \left(\frac{10 \text{ kpc}}{D} \right)^2, \quad (2)$$

where $E_{\bar{\nu}_e, \text{tot}}$ is the total energy leaving the SN in the form of $\bar{\nu}_e$ after flavor oscillations have been included, $\langle E_{\bar{\nu}_e} \rangle$ is the average $\bar{\nu}_e$ energy, and D the distance.

The energy deposited in the ice per target proton is $\mathcal{F}_{\bar{\nu}_e} \langle E_{\bar{\nu}_e} \sigma \rangle$. For the inverse β cross section we ignore weak-magnetism and recoil corrections and also the difference between $\bar{\nu}_e$ and positron energy so that [19]

$$\sigma = 9.52 \times 10^{-44} \text{ cm}^2 \left(\frac{E_{\bar{\nu}_e}}{\text{MeV}} \right)^2. \quad (3)$$

For the neutrino flux of each neutrino and anti-neutrino species we assume a distribution of the form [17]

$$F(E) = \frac{\Phi_0}{E_0} \frac{(1 + \alpha)^{1+\alpha}}{\Gamma(1 + \alpha)} \left(\frac{E}{E_0} \right)^\alpha \exp \left[-(\alpha + 1) \frac{E}{E_0} \right], \quad (4)$$

where E_0 is the average energy, α a parameter that typically takes on values 2.5–5 depending on the flavor and the phase of neutrino emission, and Φ_0 the overall flux at the detector in units of $\text{cm}^{-2} \text{ s}^{-1}$. This distribution implies

$$\langle E_{\bar{\nu}_e}^3 \rangle = \frac{(3 + \alpha)(2 + \alpha)}{(1 + \alpha)^2} \langle E_{\bar{\nu}_e} \rangle^3 = \frac{15}{8} \langle E_{\bar{\nu}_e} \rangle^3 \text{ for } \alpha = 3. \quad (5)$$

Altogether we thus find

$$\langle E_{\bar{\nu}_e} \sigma \rangle = 6.024 \times 10^{-40} \text{ MeV cm}^2 f_\sigma \quad (6)$$

with

$$f_\sigma \equiv \frac{8(3+\alpha)(2+\alpha)}{15(1+\alpha)^2} \left(\frac{\langle E_{\bar{\nu}_e} \rangle}{15 \text{ MeV}} \right)^3. \quad (7)$$

This fudge factor can also be taken to include deviations from the simplified energy dependence of the cross section and deviations from the assumed spectral shape.

The Cherenkov angle for photon emission by a charged particle is $\cos \Theta = (n\beta)^{-1}$ where n is the medium's refractive index and β the particle's velocity. With $n = 1.31$ for ice, neglecting the λ -dependence, and $\beta = 1$ we have $\Theta = 40.2^\circ$. A particle with unit charge produces Cherenkov photons per unit path length and per unit wavelength band according to

$$\frac{d^2 N_\gamma}{dx d\lambda} = \frac{2\pi\alpha \sin^2 \Theta}{\lambda^2}, \quad (8)$$

where $\alpha = 1/137$ is the fine-structure constant. Assuming that n and thus Θ are independent of wavelength we integrate over λ and find

$$\left. \frac{dN_\gamma}{dx} \right|_\lambda^\infty = 638 \text{ cm}^{-1} \frac{300 \text{ nm}}{\lambda}. \quad (9)$$

Taking the useful wavelength range to be 300–600 nm this translates into 319 photons per cm pathlength. Taking the positron mean free path to be 12 cm for an energy of 20 MeV, and taking it to be proportional to its energy, the number of useful Cherenkov photons per deposited neutrino energy is

$$\frac{N_\gamma}{E_{\bar{\nu}_e}} = 191 \text{ MeV}^{-1} f_{\text{Ch}} \quad (10)$$

with yet another fudge factor f_{Ch} .

The density of ice is 0.924 g cm^{-3} , corresponding to about $6.18 \times 10^{22} \text{ cm}^{-3}$ proton targets. Therefore, the SN neutrinos produce $1.241 \times 10^{-3} \text{ cm}^{-3} f_{\text{SN}} f_\sigma f_{\text{Ch}}$ useful Cherenkov photons per unit volume of ice. Multiplying this number with the speed of light and dividing by 4π gives us the resulting diffuse photon flux in units of $\text{cm}^{-2} \text{ s}^{-1} \text{ ster}^{-1}$. However, the average lifetime of these photons is cR_{abs} with R_{abs} the absorption length. Therefore, the neutrino-induced photon fluence is found by multiplying the flux with cR_{abs} ,

$$\frac{d\mathcal{F}_\gamma}{d\Omega} = 0.9874 \text{ cm}^{-2} \text{ ster}^{-1} f_{\text{SN}} f_\sigma f_{\text{Ch}} f_{\text{abs}} \quad (11)$$

where $f_{\text{abs}} = R_{\text{abs}}/100 \text{ m}$.

The number of events produced by this fluence in a given OM depends on the average quantum efficiency taken to be $Q = 0.20$. In addition, it depends on the angular acceptance, i.e. the effective photo cathode detection area A_{cat} times the angular acceptance range Ω_{acc} . Therefore, in one OM we expect

$$N_{\text{events}} = 310 f_{\text{SN}} f_\sigma f_{\text{Ch}} f_{\text{abs}} f_{\text{OM}} \quad (12)$$

with

$$f_{\text{OM}} = \frac{Q}{0.20} \frac{A_{\text{cat}}}{250 \text{ cm}^2} \frac{\Omega_{\text{acc}}}{2\pi}. \quad (13)$$

This result is independent of the presence of bubbles in the ice that scatter the photons. The Cherenkov glow of the ice represents an isotropic and homogeneous distribution that is not changed by elastic scattering.

2.2. Comparing With Previous Work

In order to compare our result with the one derived in Ref. [6] we need to translate their assumptions into our fudge factors. The $\bar{\nu}_e$ distribution was taken to follow a Fermi-Dirac spectrum with $T = 4$ MeV, implying $\langle E_{\bar{\nu}_e} \rangle = 12.61$ MeV. The distance of the SN was taken to be 10 kpc, and the total energy release was scaled to the Kamiokande II signal for SN 1987A. With our choice of the β cross section these assumptions correspond to $E_{\bar{\nu}_e, \text{tot}} = 3.17 \times 10^{52}$ erg, i.e. to $f_{\text{SN}} = 0.754$. These authors also used a quadratic energy dependence of the cross section. Integrating over their Fermi-Dirac spectrum they effectively used $f_{\sigma} = 0.663$. Further, they assumed 3000 useful Cherenkov photons for 20 MeV deposited energy, i.e. effectively $f_{\text{Ch}} = 0.785$. For the absorption length they used 300 m, i.e. $f_{\text{abs}} = 3$. Finally, they assumed a quantum efficiency of 25%, a cathode area of 280 cm², and an acceptance range of 2π , i.e. $f_{\text{OM}} = 1.12$. Altogether, we find for these assumptions $N_{\text{events}} = 409$ per OM. This compares with 273 in Ref. [6], i.e. our result is larger by a factor 1.5.

The result in Ref. [6] was backed up by a detailed Monte Carlo treatment of the production and propagation of Cherenkov photons in the AMANDA detector. Therefore, the difference may well relate to details of the OM acceptance and wavelength-dependent quantum efficiency and photon propagation. Many of these details will be different in IceCube where 10 inch photomultiplier tubes and different regions of ice will be used. Detailed values for the detector-dependent fudge factors must be determined specifically for IceCube once it has been built. The main difference between the assumptions in Ref. [6] and our estimate is the absorption length. When using AMANDA as a SN observatory a realistic value was taken to be around 100 m [7]. The vast difference between these estimates is that the former was based on the measured absorption length in a dust-free region of the ice. For our further estimates we stick to 100 m as a conservative assumption.

2.3. Event Rate vs. Neutrino Luminosity

In our derivation we have used the time-integrated neutrino flux, amounting to the assumption of a stationary situation. The absorption time for photons is very small, $\tau_{\text{abs}} = R_{\text{abs}}/c = 0.33 \mu\text{s} R_{\text{abs}}/100 \text{ m}$. The SN signal will vary on time scales exceeding 10 ms. Therefore, the Cherenkov glow of the ice follows the time-variation of the SN signal without discernible inertia. Hence one may replace the neutrino fluence with a time-dependent flux and N_{events} with an event rate Γ_{events} .

Moreover, for our further discussion it will be useful to consolidate our fudge-factors into one describing the detector response, and others characterizing the neutrino flux.

Therefore, we summarize our prediction for the event rate per OM in the form

$$\Gamma_{\text{events}} = 62 \text{ s}^{-1} \frac{L_{\bar{\nu}_e}}{10^{52} \text{ erg s}^{-1}} \left(\frac{10 \text{ kpc}}{D} \right)^2 f_{\text{flux}} f_{\text{det}} \quad (14)$$

where $L_{\bar{\nu}_e}$ is the $\bar{\nu}_e$ luminosity after flavor oscillations and

$$f_{\text{flux}} = \frac{15 \text{ MeV}}{\langle E_{\bar{\nu}_e} \rangle} \frac{8 \langle E_{\bar{\nu}_e}^3 \rangle}{15 (15 \text{ MeV})^3}, \quad (15)$$

$$f_{\text{det}} = f_{\text{Ch}} \frac{R_{\text{abs}}}{100 \text{ m}} \frac{Q}{0.20} \frac{A_{\text{cat}}}{250 \text{ cm}^2} \frac{\Omega_{\text{acc}}}{2\pi}. \quad (16)$$

Here, f_{det} also includes corrections for the energy dependence of the β cross section.

We stress that our simple estimate of the counting rate primarily serves the purpose of determining its magnitude relative to the background. The important feature is that the signal relative to the background can be determined with a good statistical precision. Of course, for an absolute detector calibration a detailed modeling would be necessary. For our present purpose, however, even an uncertainty of several 10% in our estimated counting rate is irrelevant.

2.4. Supernova Signal in IceCube

IceCube will have 4800 OMs so that one expects a total event number of 1.50×10^6 , taking all fudge factors to be unity. Assuming a background counting rate of 300 Hz per OM over as much as 10 s this compares with a background rate of 1.44×10^7 . Assuming Poisson fluctuations, the uncertainty of this number is 3.8×10^3 , i.e. 0.25% of the SN signal. Therefore, one can determine the SN signal with a statistical sub-percent precision, ignoring for now problems of absolute detector calibration.

In order to illustrate the statistical power of IceCube to observe a SN signal we use two different numerical SN simulations. The first was performed by the Livermore group [20] that involves traditional input physics for mu- and tau-neutrino interactions and a flux-limited diffusion scheme for treating neutrino transport. The great advantage of this simulation is that it covers the full evolution from infall over the explosion to the Kelvin-Helmholtz cooling phase of the newly formed neutron star. We show the Livermore $\bar{\nu}_e$ and $\bar{\nu}_x$ lightcurves in Fig 1 (left panels). Here and in the following we take $\bar{\nu}_x$ to stand for either $\bar{\nu}_\mu$ or $\bar{\nu}_\tau$. Apart from very small differences the SN fluxes and spectra are thought to be equal for ν_μ , ν_τ , $\bar{\nu}_\mu$, and $\bar{\nu}_\tau$.

Our second simulation was performed with the Garching code [21]. It includes all relevant neutrino interaction rates, including nucleon bremsstrahlung, neutrino pair processes, weak magnetism, nucleon recoils, and nuclear correlation effects. The neutrino transport part is based on a Boltzmann solver. The neutrino-radiation hydrodynamics program allows one to perform spherically symmetric as well as multi-dimensional simulations. The progenitor model is a $15 M_\odot$ star with a $1.28 M_\odot$ iron core. The period from shock formation to 468 ms after bounce was evolved in two dimensions. The subsequent evolution of the model is simulated in spherical symmetry. At 150 ms the explosion sets in, although a small modification of the Boltzmann transport was

necessary to allow this to happen [22]. Unmanipulated full-scale models with an accurate treatment of the microphysics currently do not obtain explosions [23]. This run will be continued beyond the current epoch of 750 ms post bounce; we here use the preliminary results currently available [18]. We show the Garching $\bar{\nu}_e$ and $\bar{\nu}_x$ lightcurves in Fig 1 (right panels).

We take the Livermore simulation to represent traditional predictions for flavor-dependent SN neutrino fluxes and spectra that were used in many previous discussions of SN neutrino oscillations. The Garching simulation is taken to represent a situation when the $\bar{\nu}_x$ interactions are more systematically included so that the flavor-dependent spectra and fluxes are more similar than had been assumed previously [15, 16, 17, 18]. We think it is useful to juxtapose the IceCube response for both cases.

Another difference is that in Livermore the accretion phase lasts longer. Since the explosion mechanism is not finally settled, it is not obvious which case is more realistic. Moreover, there could be differences between different SNe. The overall features are certainly comparable between the two simulations.

In Fig. 2 we show the expected counting rates in IceCube on the basis of Eq. (14) for an assumed distance of 10 kpc and 4800 OM for the Livermore (left) and Garching (right) simulations. We also show this signal in 50 ms bins where we have added noise from a background of 300 Hz per OM. The baseline is at the average background rate so that negative counts correspond to downward background fluctuations.

One could easily identify the existence and duration of the accretion phase and thus test the standard delayed-explosion scenario. One could also measure the overall duration of the cooling phase and thus exclude the presence of significant exotic energy losses. Therefore, many of the particle-physics limits based on the SN 1987A neutrinos [24] could be supported with a statistically serious signal. If the SN core were to collapse to a black hole after some time, the sudden turn-off of the neutrino flux could be identified. In short, when a galactic SN occurs, IceCube is a powerful stand-alone neutrino detector, providing us with a plethora of information that is of fundamental astrophysical and particle-physics interest.

In addition, IceCube is extremely useful as a co-detector with another high-statistics observatory to measure neutrino oscillation effects, a topic that we now explore.

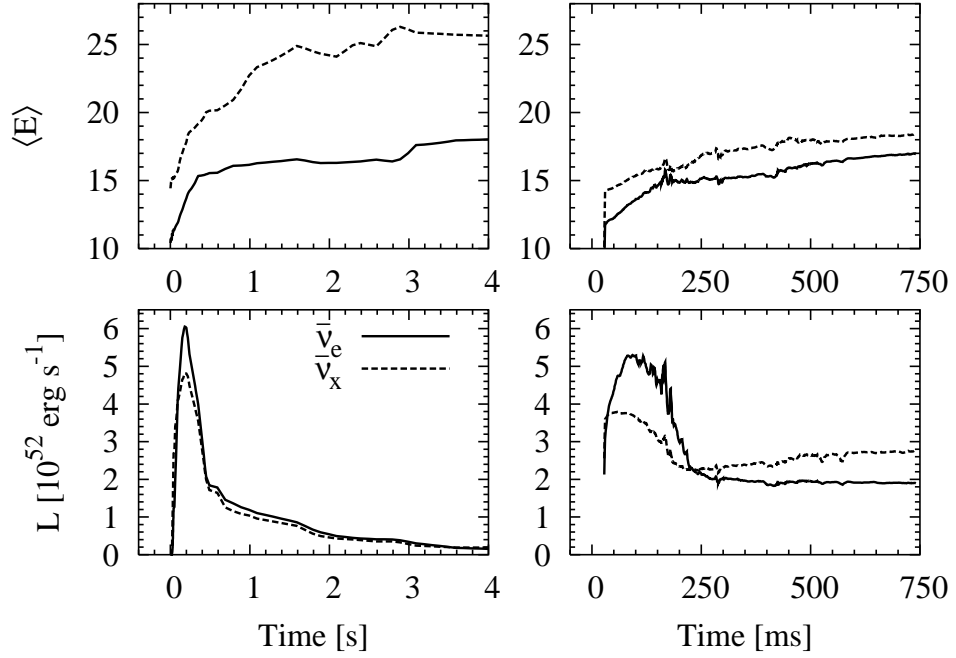


Figure 1. Supernova $\bar{\nu}_e$ and $\bar{\nu}_x$ light curves and average energies. *Left:* Livermore simulation [20]. *Right:* Garching simulation [18].

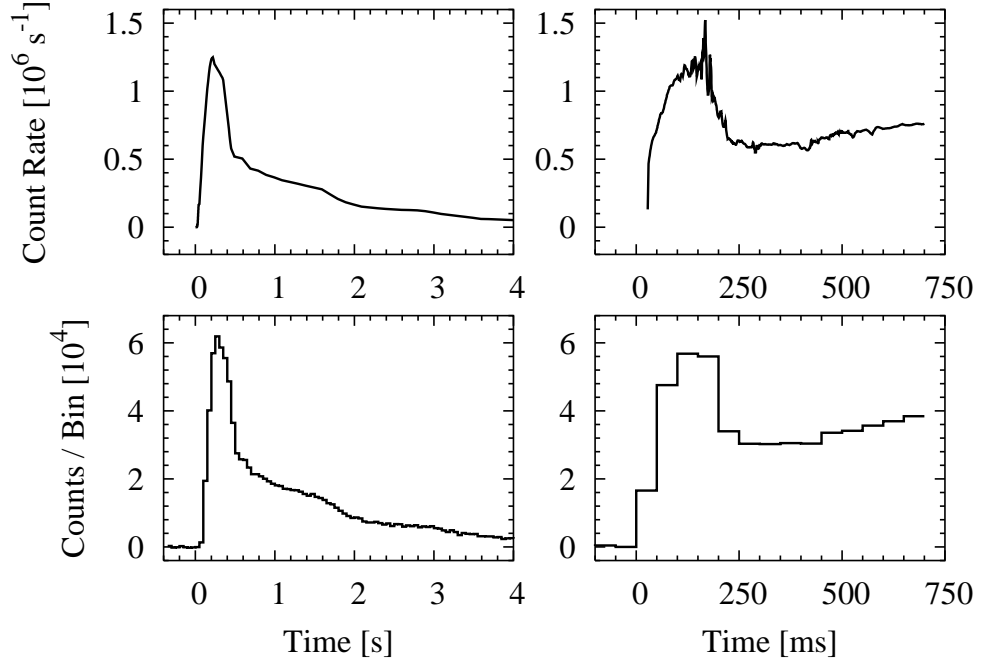


Figure 2. Supernova signal in IceCube assuming a distance of 10 kpc, based on the Livermore simulation (left) and the Garching one (right), in both cases ignoring flavor oscillations. In the bottom panels we have used 50 ms bins and have added noise from a background rate of 300 Hz per OM.

3. Observing Supernova Neutrinos Through The Earth

3.1. Earth Matter Effect on SN Neutrino Spectra

Neutrino oscillations are now firmly established by measurements of solar and atmospheric neutrinos and the KamLAND and K2K long-baseline experiments [25, 26, 27, 28, 29, 30]. Evidently the weak interaction eigenstates ν_e , ν_μ and ν_τ are non-trivial superpositions of three mass eigenstates ν_1 , ν_2 and ν_3 ,

$$\begin{pmatrix} \nu_e \\ \nu_\mu \\ \nu_\tau \end{pmatrix} = U \begin{pmatrix} \nu_1 \\ \nu_2 \\ \nu_3 \end{pmatrix}, \quad (17)$$

where U is the leptonic mixing matrix that can be written in the canonical form

$$U = \begin{pmatrix} 1 & 0 & 0 \\ 0 & c_{23} & s_{23} \\ 0 & -s_{23} & c_{23} \end{pmatrix} \begin{pmatrix} c_{13} & 0 & e^{i\delta} s_{13} \\ 0 & 1 & 0 \\ -e^{-i\delta} s_{13} & 0 & c_{13} \end{pmatrix} \begin{pmatrix} c_{12} & s_{12} & 0 \\ -s_{12} & c_{12} & 0 \\ 0 & 0 & 1 \end{pmatrix}. \quad (18)$$

Here $c_{12} = \cos \theta_{12}$ and $s_{12} = \sin \theta_{12}$ etc., and δ is a phase that can lead to CP-violating effects, that are, however, irrelevant for SN neutrinos.

The mass squared differences relevant for the atmospheric and solar neutrino oscillations obey a hierarchy $\Delta m_{\text{atm}}^2 \gg \Delta m_{\odot}^2$. This hierarchy, combined with the observed smallness of the angle θ_{13} at CHOOZ [31] implies that the atmospheric neutrino oscillations essentially decouple from the solar ones and each of these is dominated by only one of the mixing angles. The atmospheric neutrino oscillations are controlled by θ_{23} that may well be maximal (45°). The solar case is dominated by θ_{12} , that is large but not maximal. From a global 3-flavor analysis of all data one finds the 3σ ranges for the mass differences $\Delta m_{ij}^2 \equiv m_i^2 - m_j^2$ and mixing angles summarized in Table 1.

Table 1. Neutrino mixing parameters from a global analysis of all experiments (3σ ranges) [25].

Observation	Mixing angle	Δm^2 [meV ²]
Sun, KamLAND	$\theta_{12} = 27^\circ\text{--}42^\circ$	$\Delta m_{21}^2 = 55\text{--}190$
Atmosphere, K2K	$\theta_{23} = 32^\circ\text{--}60^\circ$	$ \Delta m_{32}^2 = 1400\text{--}6000$
CHOOZ	$\theta_{13} < 14^\circ$	$\Delta m_{31}^2 \approx \Delta m_{32}^2$

A SN core is essentially a neutrino blackbody source, but small flavor-dependent differences of the fluxes and spectra remain. We denote the fluxes of $\bar{\nu}_e$ and ν_x at Earth that would be observable in the absence of oscillations by F_e^0 and F_x^0 , respectively. In the presence of oscillations a $\bar{\nu}_e$ detector actually observes

$$F_e^D(E) = \bar{p}^D(E) F_e^0(E) + [1 - \bar{p}^D(E)] F_x^0, \quad (19)$$

where $\bar{p}^D(E)$ is the $\bar{\nu}_e$ survival probability after propagation through the SN mantle and perhaps part of the Earth before reaching the detector.

A significant modification of the survival probability due to the propagation through the Earth appears only for those combinations of neutrino mixing parameters shown in Table 2. The Earth matter effect depends strongly on two parameters, the sign of Δm_{32}^2 and the value of $|\theta_{13}|$ [10, 11]. The “normal hierarchy” corresponds to $m_1 < m_2 < m_3$, i.e. $\Delta m_{32}^2 > 0$, whereas the “inverted hierarchy” corresponds to $m_3 < m_1 < m_2$, i.e. $\Delta m_{32}^2 < 0$. Note that the presence or absence of the Earth effect discriminates between values of $\sin^2 \theta_{13}$ less or greater than 10^{-3} , i.e. θ_{13} less or larger than about 1.8° . Thus, the Earth effect is sensitive to values of θ_{13} that are much smaller than the current limit.

Table 2. The Earth effect appears for the indicated flavors in a SN signal.

13-Mixing	Normal Hierarchy	Inverted Hierarchy
$\sin^2 \theta_{13} \lesssim 10^{-3}$	ν_e and $\bar{\nu}_e$	ν_e and $\bar{\nu}_e$
$\sin^2 \theta_{13} \gtrsim 10^{-3}$	$\bar{\nu}_e$	ν_e

Let us consider those scenarios where the mass hierarchy and the value of θ_{13} are such that the Earth effect appears for $\bar{\nu}_e$. In such cases the $\bar{\nu}_e$ survival probability $\bar{p}^D(E)$ is given by

$$\bar{p}^D \approx \cos^2 \theta_{12} - \sin 2\bar{\theta}_{e2}^\oplus \sin(2\bar{\theta}_{e2}^\oplus - 2\theta_{12}) \sin^2 \left(12.5 \frac{\overline{\Delta m_\oplus^2} L}{E} \right), \quad (20)$$

where the energy dependence of all quantities will always be implicit. Here $\bar{\theta}_{e2}^\oplus$ is the mixing angle between $\bar{\nu}_e$ and $\bar{\nu}_2$ in Earth matter while $\overline{\Delta m_\oplus^2}$ is the mass squared difference between the two anti-neutrino mass eigenstates $\bar{\nu}_1$ and $\bar{\nu}_2$ in units of 10^{-5}eV^2 , L is the distance traveled through the Earth in units of 1000 km, and E is the neutrino energy in MeV. We have assumed a constant matter density inside the Earth, which is a good approximation for $L < 10.5$, i.e. as long as the neutrinos do not pass through the core of the Earth.

3.2. Magnitude of Observable Effect at IceCube

In order to calculate the extent of the Earth effect for IceCube, we will assume that the relevant mixing parameters are $\Delta m_{12}^2 = 6 \times 10^{-5} \text{eV}^2$ and $\sin^2(2\theta_{12}) = 0.9$. We further assume that the source spectra are given by the functional form Eq. (4). The values of the parameters α and $\langle E \rangle$ for both the $\bar{\nu}_e$ and $\bar{\nu}_x$ spectra are in general time dependent.

In Fig. 3 we show the variation of the expected IceCube signal with Earth-crossing length L for the two sets of parameters detailed in Table 3. The first could be representative of the accretion phase, the second of the cooling signal. We use the two-density approximation for the Earth density profile, where the core has a density of 11.5 g cm^{-3} and a radius of 3500 km, while the density of the Earth mantle was taken to be 4.5 g cm^{-3} . We observe that for short distances, corresponding to near-horizontal neutrino trajectories, the signal varies strongly with L . Between about 3,000 and 10,500 km it reaches an asymptotic value that we call the “asymptotic mantle

value.” For Case (a), this value corresponds to about 1.5% depletion of the signal, whereas for (b) it corresponds to about 6.5% depletion.

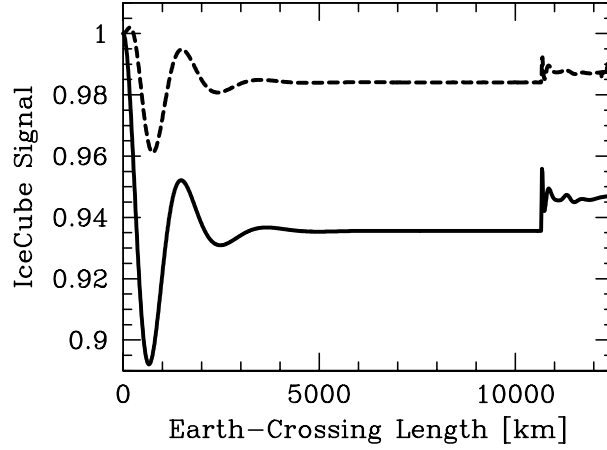


Figure 3. Variation of the expected IceCube signal with neutrino Earth crossing length L for the assumed flux and mixing parameters of Table 3. The signal is normalized to 1 when no Earth effect is present, i.e. for $L = 0$. The dashed line is for the case representing the accretion phase, the solid line for the cooling phase.

Table 3. Flux parameters for two representative cases.

Example	Phase	$\langle E_{\bar{\nu}_e} \rangle$ [MeV]	$\langle E_{\bar{\nu}_x} \rangle$ [MeV]	$\alpha_{\bar{\nu}_e}$	$\alpha_{\bar{\nu}_x}$	$\Phi_{\bar{\nu}_e}^0 / \Phi_{\bar{\nu}_x}^0$	Asymptotic Earth Effect
(a)	Accretion	15	17	4	3	1.5	−1.5%
(b)	Cooling	15	18	3	3	0.8	−6.5%

Beyond an Earth-crossing length of $\sim 10,500$ km, the neutrinos have to cross the Earth core with another large jump in density. The core effects change the asymptotic mantle value by $\sim 1\%$ as can be seen in Fig. 3. We neglect the core effects in the following analysis, and the “asymptotic value” always refers to the asymptotic mantle value.

For the largest part of the sky the Earth effect either appears with this asymptotic value (“neutrinos coming from below”), or it does not appear at all (“neutrinos from above”). Therefore, we now focus on the asymptotic value and study how the signal modification depends on the assumed flux parameters. In Table 4 we show the signal modification for $\langle E_{\bar{\nu}_e} \rangle = 15$ MeV, $\alpha_{\bar{\nu}_e} = 4.0$, and $\alpha_{\bar{\nu}_x} = 3.0$ as a function of $\langle E_{\bar{\nu}_x} \rangle$ and the flux ratio $\Phi_{\bar{\nu}_e}^0 / \Phi_{\bar{\nu}_x}^0$. In Table 5 we show the same with $\alpha_{\bar{\nu}_e} = \alpha_{\bar{\nu}_x} = 3.0$. The results are shown in the form of contour plots in Fig. 4.

Even for mildly different fluxes or spectra the signal modification is several percent, by far exceeding the statistical uncertainty of the IceCube signal, although the *absolute* calibration of IceCube may remain uncertain to within several percent. However, the signal modification will vary with time during the SN burst. During the early accretion

Table 4. Asymptotic IceCube signal modification by the Earth effect. The fixed flux parameters are $\langle E_{\bar{\nu}_e} \rangle = 15$ MeV, $\alpha_{\bar{\nu}_e} = 4.0$, and $\alpha_{\bar{\nu}_x} = 3.0$.

Flux ratio $\Phi_{\bar{\nu}_e}^0 / \Phi_{\bar{\nu}_x}^0$	$\langle E_{\bar{\nu}_x} \rangle$ [MeV]					
	15	16	17	18	19	20
2.0	1.026	1.014	1.002	0.988	0.974	0.960
1.9	1.023	1.011	0.999	0.985	0.971	0.956
1.8	1.021	1.009	0.995	0.982	0.967	0.952
1.7	1.018	1.005	0.992	0.978	0.963	0.948
1.6	1.015	1.002	0.988	0.974	0.959	0.944
1.5	1.012	0.998	0.984	0.969	0.954	0.939
1.4	1.008	0.994	0.980	0.965	0.949	0.934
1.3	1.004	0.990	0.975	0.960	0.944	0.928
1.2	1.000	0.985	0.970	0.954	0.938	0.922
1.1	0.995	0.980	0.964	0.948	0.932	0.915
1.0	0.989	0.974	0.957	0.941	0.925	0.908
0.9	0.983	0.967	0.950	0.934	0.917	0.901
0.8	0.976	0.959	0.942	0.925	0.909	0.892
0.7	0.967	0.950	0.933	0.916	0.899	0.883
0.6	0.958	0.940	0.923	0.906	0.889	0.873
0.5	0.946	0.928	0.911	0.894	0.877	0.862

Table 5. Same as Table 4 with $\alpha_{\bar{\nu}_e} = \alpha_{\bar{\nu}_x} = 3.0$.

Flux ratio $\Phi_{\bar{\nu}_e}^0 / \Phi_{\bar{\nu}_x}^0$	$\langle E_{\bar{\nu}_x} \rangle$ [MeV]					
	15	16	17	18	19	20
2.0	1.036	1.024	1.012	1.000	0.986	0.972
1.9	1.033	1.022	1.010	0.996	0.983	0.968
1.8	1.031	1.019	1.006	0.993	0.979	0.964
1.7	1.028	1.016	1.003	0.989	0.975	0.960
1.6	1.025	1.013	0.999	0.985	0.971	0.955
1.5	1.022	1.009	0.995	0.981	0.966	0.951
1.4	1.019	1.005	0.991	0.976	0.961	0.945
1.3	1.015	1.001	0.986	0.971	0.955	0.940
1.2	1.010	0.996	0.981	0.965	0.949	0.933
1.1	1.006	0.991	0.975	0.959	0.943	0.927
1.0	1.000	0.985	0.969	0.952	0.936	0.919
0.9	0.994	0.978	0.961	0.945	0.928	0.911
0.8	0.986	0.970	0.953	0.936	0.919	0.903
0.7	0.978	0.961	0.944	0.926	0.910	0.893
0.6	0.968	0.950	0.933	0.916	0.899	0.882
0.5	0.956	0.938	0.920	0.903	0.886	0.870

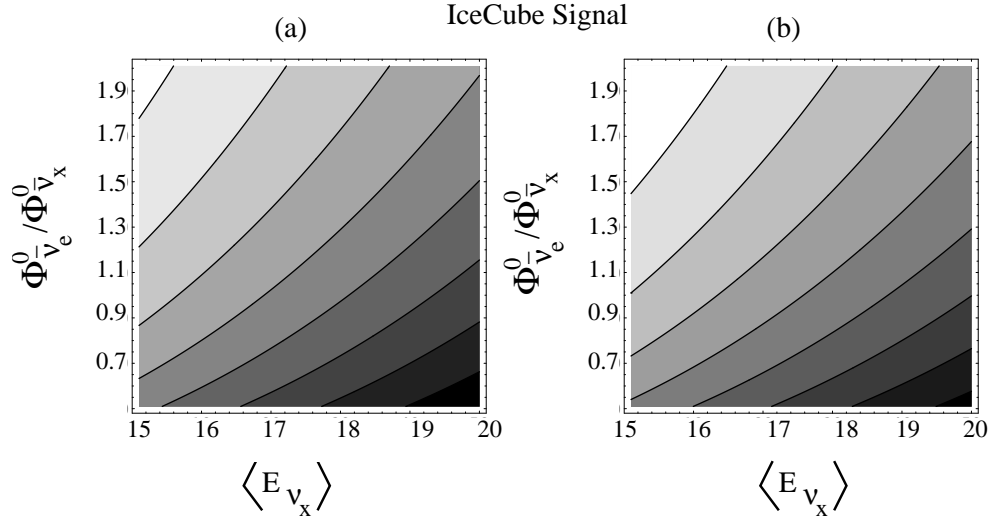


Figure 4. Asymptotic IceCube signal modification by the Earth effect. The fixed flux parameters are (a) $\langle E_{\bar{\nu}_e} \rangle = 15$ MeV, $\alpha_{\bar{\nu}_e} = 4.0$, and $\alpha_{\bar{\nu}_x} = 3.0$ and (b) $\langle E_{\bar{\nu}_e} \rangle = 15$ MeV, $\alpha_{\bar{\nu}_e} = \alpha_{\bar{\nu}_x} = 3.0$. The contours are equally spaced starting from 1.02 (light) in 0.02 decrements to smaller values (darker).

phase that is expected to last for a few 100 ms and corresponds to a significant fraction of the overall signal, the $\bar{\nu}_x$ flux may be almost a factor of 2 smaller than the $\bar{\nu}_e$ flux, but it will be slightly hotter and less pinched [18]. This corresponds to Case (a) above; it is evident from Fig. 3 and Table 4 that this implies that the Earth effect is very small. During the Kelvin-Helmholtz cooling phase the flux ratio is reversed with more $\bar{\nu}_x$ being emitted than $\bar{\nu}_e$, but still with the same hierarchy of energies. This corresponds to Case (b); in this case the Earth effect could be about 6%. This time dependence may allow one to detect the Earth effect without a precise absolute detector calibration.

In order to illustrate the time dependence of the Earth effect we show in Fig. 5 the expected counting rate in IceCube for both the Livermore (left panels) and Garching (right panels) simulations. In the upper panels we show the expected counting rate with flavor oscillations in the SN mantle, but no Earth effect (solid lines), or with the asymptotic Earth effect (dashed lines) that obtains for a large Earth-crossing path. Naturally the differences are very small so that we show in the lower panels the ratio of these curves, i.e. the expected counting rate with/without Earth effect as a function of time for both Livermore and Garching. While for the Livermore simulation there is a large Earth effect even at early times, the change from early to late times in both cases is around 4–5%. Therefore, the most model-independent signature is a time variation of the Earth effect during the SN neutrino signal.

In order to demonstrate the statistical significance of these effects we integrate the expected signal for both simulations separately for the accretion phase and the subsequent cooling phase; the results are shown in Table 6. For both simulations the Earth effect itself and its change with time is statistically highly significant. Based on the Livermore simulation, the Earth effect is much more pronounced than in Garching,

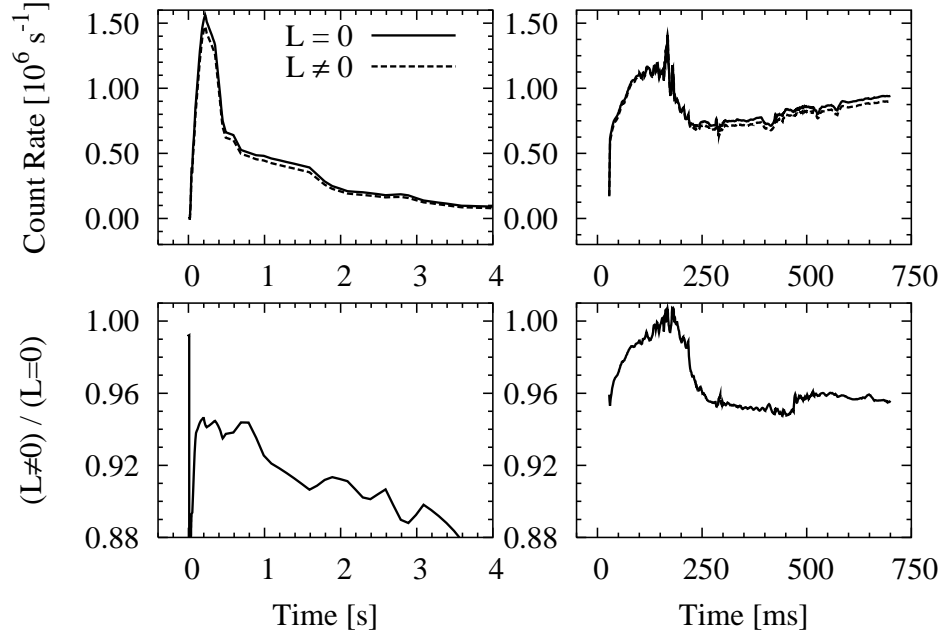


Figure 5. Earth effect in IceCube. The upper panels show the expected counting rate based on the Livermore (left) and Garching (right) models, including flavor oscillations. The solid line is without Earth effect ($L = 0$), the dashed line with asymptotic Earth effect ($L \neq 0$). The lower panels show the ratio between these curves, i.e. the ratio of counting rates with/without Earth effect.

the latter involving more up-to-date input physics for neutrino transport. However, the *difference* between the Earth effect during accretion and cooling is not vastly different between the two simulations. Recalling that the absolute detector calibration may be very uncertain so that one has to rely on the temporal variation of the Earth effect, the difference between Livermore and Garching becomes much smaller. We expect that it is quite generic that the temporal change of the Earth effect is a few percent of the overall counting rate.

Table 6. IceCube Cherenkov counts for the numerical SN models.

	Livermore		Garching	
	Accretion	Cooling	Accretion	Cooling
Integration time [s]	0–0.500	0.500–3	0–0.250	0.250–0.700
SN Signal [Counts]				
No Earth Effect	519,080	818,043	173,085	407,715
Asymptotic Earth Effect	488,093	751,137	171,310	390,252
Difference	30,987	66,906	1,775	17,463
Fractional Difference	–5.97%	–8.18%	–1.03%	–4.28%
Background [Counts]	720,000	4,320,000	360,000	648,000
$\sqrt{\text{Background}}/\text{Signal}$	0.16%	0.25%	0.35%	0.20%

3.3. Super- or Hyper-Kamiokande and IceCube

One can measure the Earth effect in IceCube only in conjunction with another high-statistics detector. We do not attempt to simulate in detail the SN signal in this other detector but simply assume that it can be measured with a precision at least as good as in IceCube. One candidate is Super-Kamiokande, a water Cherenkov detector that would measure around 10^4 events from a galactic SN at a distance of 10 kpc. Therefore, the statistical precision for the total neutrino energy deposition in the water is around 1% and thus worse than in IceCube. Even though Super-Kamiokande will measure a larger number of Cherenkov photons than IceCube, a single neutrino event will cause an entire Cherenkov ring to be measured, i.e. the photons are highly correlated. Therefore, in the estimated statistical \sqrt{N} fluctuation of the signal, the fluctuating number N is that of the detected neutrinos. If the future Hyper-Kamiokande is built, its fiducial volume would be about 30 times that of Super-Kamiokande. In this case the statistical signal precision exceeds that of IceCube for the equivalent observable.

We denote the equivalent IceCube signal measured by Super- or Hyper-Kamiokande as N_{SK} and the IceCube signal as N_{IC} . If the distances traveled by the neutrinos before reaching these two detectors are different, the Earth effect on the neutrino spectra may be different, which will reflect in the ratio $N_{\text{SK}}/N_{\text{IC}}$. Of course, in the absence of the Earth effect this ratio equals unity by definition.

The geographical position of IceCube with respect to Super- or Hyper-Kamiokande at a latitude of 36.4° is well-suited for the detection of the Earth effect through a combination of the signals. Using Fig. 3 we can already draw some qualitative conclusions about the ratio $N_{\text{SK}}/N_{\text{IC}}$. Clearly, $N_{\text{SK}}/N_{\text{IC}} = 1$ if neutrinos do not travel through the Earth before reaching either detector. If the distance traveled by neutrinos through the Earth is more than 3000 km for both detectors, the Earth effects on both N_{SK} and N_{IC} are nearly equal and their ratio stays around unity. If the neutrinos come “from above” for SK and “from below” for IceCube, or vice versa, the Earth matter effect will shift this ratio from unity.

In Fig. 6, we show contours of $N_{\text{SK}}/N_{\text{IC}}$ for the SN position in terms of the location on Earth where the SN is at the zenith. The map is an area preserving Hammer-Aitoff projection so that the sizes of different regions in the figure gives a realistic idea of the “good” and “bad” regions of the sky. In order to generate the contours we use the parameters of Case (b) in Table 3 so that the asymptotic suppression of the signal is about 6.5%. The sky falls into four distinct regions depending on the direction of the neutrinos relative to either detector as described in Table 7. When the neutrinos come from above for both detectors (Region D) there is no Earth effects. If they come from below in both (Region C), the Earth effect is large in both. Depending on the exact distance traveled through the Earth, the event ratio can be large, but generally fluctuates around 1. In the other regions where the neutrinos come from above for one detector and from below for the other (Regions A and B) the relative effect is large.

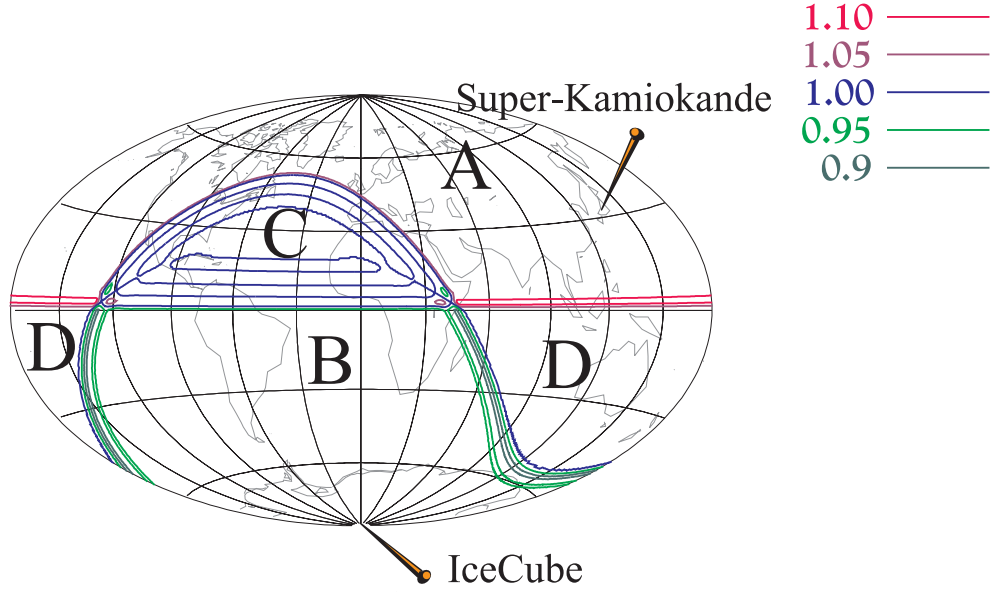


Figure 6. Contours of $N_{\text{SK}}/N_{\text{IC}}$ on the map of the sky projected on the Earth. The regions A, B, C, D are described in Table 7.

Table 7. Regions in Fig. 6 for the Earth effect in IceCube and Super-Kamiokande.

Region	Sky fraction	Neutrinos come from		$N_{\text{SK}}/N_{\text{IC}}$
		IceCube	Super-K	
A	0.35	below	above	1.070
B	0.35	above	below	0.935
C	0.15	below	below	Fluctuations around 1
D	0.15	above	above	1

4. Conclusions

For assumptions about the flavor-dependent SN neutrino fluxes and spectra that agree with state-of-the-art studies, the Earth matter effect on neutrino oscillations shows up in the IceCube signal of a future galactic SN on the level of a few percent. If the IceCube signal can be compared with another high-statistics signal, notably in Super-Kamiokande or Hyper-Kamiokande, the Earth effect becomes clearly visible as a difference between the detectors. As one is looking for a signal modification in the range of a few percent, the absolute detector calibration may not be good enough in one or both of the instruments. However, for typical numerical SN simulations the effect is time dependent and most notably differs between the early accretion phase and the subsequent neutron star cooling phase. Therefore, one would have to search for a temporal variation of the relative detector signals of a few percent. The large number of optical modules in IceCube renders this task statistically possible. In fact depending on the differences in flavor-dependent fluxes, the statistical accuracy of Super-Kamiokande

may turn out to be the limiting factor. This limitation is not significant for Hyper-Kamiokande.

The unique location of IceCube in Antarctica implies that for a large portion of the sky this detector sees the SN through the Earth when Super- and Hyper-Kamiokande sees it from above, or the other way round, i.e. the chances of a relative signal difference between the detectors are large. If both detectors were to see the SN from above there would be no Earth effect to detect.

Assuming that the magnitude of the mixing angle θ_{13} can be established to be large in the sense of $\sin^2 \theta_{13} \gtrsim 10^{-3}$ by a long-baseline experiment [32, 33, 34], observing the Earth effect in SN anti-neutrinos implies the normal mass hierarchy. On the other hand, if $\sin^2 \theta_{13} \lesssim 10^{-3}$ has been established, the Earth effect is unavoidable. Not observing it would imply that the primary SN neutrino fluxes and spectra are more similar than indicated by state-of-the-art numerical simulations.

If $\sin^2 \theta_{13} \gtrsim 10^{-3}$ is known, and we do not observe the Earth effect, it still does not prove the inverted mass hierarchy. It could also mean that we do not properly understand the flavor-dependent source fluxes and spectra. Therefore, even if $\sin^2 \theta_{13} \gtrsim 10^{-3}$ is known, our method only allows one to detect the normal mass hierarchy, it does not strictly allow one to exclude it. As far as neutrino parameters are concerned, only a positive detection of the Earth effect would count for much. Of course, a normal mass hierarchy and $\sin^2 \theta_{13} \gtrsim 10^{-3}$ is certainly a plausible scenario so that expecting a positive identification of the Earth effect is not a far-fetched possibility.

In summary, even though galactic SNe are rare, the anticipated longevity of IceCube and the long-term neutrino program at Super- or Hyper-Kamiokande imply that detecting the Earth effect in a SN neutrino burst is certainly a distinct possibility. This could identify the normal neutrino mass hierarchy, a daunting task at long-baseline experiments [32, 33, 34]. Given the difficulty of pinning down the mass hierarchy at long-baseline experiments, both IceCube and Super- or Hyper-Kamiokande should take all instrumental and experimental steps required to ensure the feasibility of a high-statistics simultaneous SN observation.

Acknowledgments

This work was supported, in part, by the Deutsche Forschungsgemeinschaft under grant No. SFB-375 and by the European Science Foundation (ESF) under the Network Grant No. 86 Neutrino Astrophysics. We thank Francis Halzen and Robert Buras for helpful comments on an early version of this manuscript.

References

- [1] C. Wiebusch *et al.* [AMANDA Collaboration], “Results from Amanda,” *Mod. Phys. Lett. A* **17**, 2019 (2002).
- [2] Amanda, <http://amanda.physics.wisc.edu/>
- [3] J. Ahrens *et al.* [IceCube Collaboration], “IceCube: The next generation neutrino telescope at the South Pole,” *astro-ph/0209556*.
- [4] IceCube, <http://icecube.wisc.edu/>
- [5] F. Halzen, J. E. Jacobsen and E. Zas, “Possibility that high-energy neutrino telescopes could detect supernovae,” *Phys. Rev. D* **49**, 1758 (1994).
- [6] F. Halzen, J. E. Jacobsen and E. Zas, “Ultra-transparent antarctic ice as a supernova detector,” *Phys. Rev. D* **53**, 7359 (1996) [*astro-ph/9512080*].
- [7] J. Ahrens *et al.* [AMANDA Collaboration], “Search for supernova neutrino-bursts with the AMANDA detector,” *Astropart. Phys.* **16**, 345 (2002) [*astro-ph/0105460*].
- [8] K. Scholberg, “SNEWS: The Supernova early warning system,” *astro-ph/9911359*.
- [9] SNEWS: The SuperNova Early Warning System, <http://hep.bu.edu/~snnet/>
- [10] A. S. Dighe and A. Y. Smirnov, “Identifying the neutrino mass spectrum from the neutrino burst from a supernova,” *Phys. Rev. D* **62**, 033007 (2000) [*hep-ph/9907423*].
- [11] A. S. Dighe, “Earth matter effects on the supernova neutrino spectra,” *hep-ph/0106325*.
- [12] C. Lunardini and A. Y. Smirnov, “Supernova neutrinos: Earth matter effects and neutrino mass spectrum,” *Nucl. Phys. B* **616**, 307 (2001) [*hep-ph/0106149*].
- [13] C. Lunardini and A. Y. Smirnov, “Probing the neutrino mass hierarchy and the 13-mixing with supernovae,” *hep-ph/0302033*.
- [14] K. Takahashi and K. Sato, “Earth effects on supernova neutrinos and their implications for neutrino parameters,” *Phys. Rev. D* **66**, 033006 (2002) [*hep-ph/0110105*].
- [15] G. G. Raffelt, “Mu- and tau-neutrino spectra formation in supernovae,” *Astrophys. J.* **561**, 890 (2001) [*astro-ph/0105250*].
- [16] R. Buras, H. T. Janka, M. T. Keil, G. G. Raffelt and M. Rampp, “Electron-neutrino pair annihilation: A new source for muon and tau neutrinos in supernovae,” *Astrophys. J.* **587**, 320 (2003) [*astro-ph/0205006*].
- [17] M. T. Keil, G. G. Raffelt and H. T. Janka, “Monte Carlo study of supernova neutrino spectra formation,” *Astrophys. J.*, in press (2003) [*astro-ph/0208035*].
- [18] G. G. Raffelt, M. Th. Keil, R. Buras, H.-T. Janka and M. Rampp, “Supernova neutrinos: Flavor-dependent fluxes and spectra,” *Proc. NOON 03* (10–14 February 2003, Kanazawa, Japan), *astro-ph/0303226*.
- [19] P. Vogel and J. F. Beacom, “Angular distribution of neutron inverse beta decay, $\bar{\nu}_e + p \rightarrow e^+ n$,” *Phys. Rev. D* **60**, 053003 (1999) [*hep-ph/9903554*].
- [20] T. Totani, K. Sato, H. E. Dalhed and J. R. Wilson, “Future detection of supernova neutrino burst and explosion mechanism,” *Astrophys. J.* **496**, 216 (1998) [*astro-ph/9710203*].
- [21] M. Rampp and H.-T. Janka, “Radiation hydrodynamics with neutrinos: Variable Eddington factor method for core-collapse supernova simulations”, *Astron. Astrophys.* **396**, 361 (2002) [*astro-ph/0203101*].
- [22] H.-T. Janka, R. Buras, K. Kifonidis, T. Plewa and M. Rampp, “Explosion Mechanisms of Massive Stars”, in: *Core Collapse of Massive Stars*, edited by C.L. Fryer (Kluwer Academic Publ., Dordrecht, 2003) [*astro-ph/0212314*].
- [23] R. Buras, M. Rampp, H.-T. Janka and K. Kifonidis, “Improved models of stellar core collapse and still no explosions: What is missing?”, *Physical Review Letters*, submitted (2003) [*astro-ph/0303171*].
- [24] G. G. Raffelt, “Particle physics from stars,” *Ann. Rev. Nucl. Part. Sci.* **49**, 163 (1999) [*hep-ph/9903472*].
- [25] M. C. Gonzalez-Garcia and Y. Nir, “Developments in neutrino physics,” *hep-ph/0202058*.

- [26] G. L. Fogli, E. Lisi, A. Marrone, D. Montanino, A. Palazzo and A. M. Rotunno, “Solar neutrino oscillation parameters after first KamLAND results,” *Phys. Rev. D* **67**, 073002 (2003) [hep-ph/0212127].
- [27] J. N. Bahcall, M. C. Gonzalez-Garcia and C. Peña-Garay, “Solar neutrinos before and after KamLAND,” *JHEP* **02**, 009 (2003) [hep-ph/0212147].
- [28] P. C. de Holanda and A. Y. Smirnov, “LMA MSW solution of the solar neutrino problem and first KamLAND results,” *JCAP* **02**, 001 (2003) [hep-ph/0212270].
- [29] M. Maltoni, T. Schwetz and J. W. Valle, “Combining first KamLAND results with solar neutrino data,” *Phys. Rev. D* **67**, 093003 (2003) [hep-ph/0212129].
- [30] M. Maltoni, T. Schwetz, M. A. Tortola and J. W. Valle, “Constraining neutrino oscillation parameters with current solar and atmospheric data,” *Phys. Rev. D* **67**, 013011 (2003) [hep-ph/0207227].
- [31] M. Apollonio *et al.* [CHOOZ Collaboration], “Limits on neutrino oscillations from the CHOOZ experiment,” *Phys. Lett. B* **466**, 415 (1999) [hep-ex/9907037].
- [32] V. D. Barger, S. Geer, R. Raja and K. Whisnant, “Exploring neutrino oscillations with superbeams,” *Phys. Rev. D* **63**, 113011 (2001) [hep-ph/0012017].
- [33] A. Cervera, A. Donini, M. B. Gavela, J. J. Gomez Cadenas, P. Hernandez, O. Mena and S. Rigolin, “Golden measurements at a neutrino factory,” *Nucl. Phys. B* **579**, 17 (2000); Erratum *ibid.* **593**, 731 (2001) [hep-ph/0002108].
- [34] M. Freund, P. Huber and M. Lindner, “Systematic exploration of the neutrino factory parameter space including errors and correlations,” *Nucl. Phys. B*, **615**, 331 (2001) [hep-ph/0105071].